A model of the X-ray response of the ACIS CCD

G. Prigozhin[a], A. Rasmussen[b], M. Bautz[a], G. Ricker[a]

[a]Massachusetts Institute of Technology, Center for Space Research, Cambridge, MA

[b]Columbia University, Columbia Astrophysics Laboratory, New York

ABSTRACT

We have developed a comprehensive model of the response of a CCD to soft X-ray illumination. The model is based on the Monte Carlo technique and follows the interactions with the device material of individual photons thrown into the structure, calculating device reaction to each of them. It incorporates a very detailed description of the CCD gate structure, as well as accurately measured absorption coefficients. The fluorescent and escape peak model takes into account interactions inside the gate structure, which dramatically improves the agreement with the experimental data at energies close to the Si absorption edge. The shape of the low energy tail is simulated according to our new model of electron cloud charge splitting at the interface between Si and SiO_2. An origin of the tail in the horizontally split events is explained as coming from the $p+$ area in the channel stop region and is modeled accordingly.

Keywords: charge coupled devices, response function, X-rays, quantum efficiency

1. INTRODUCTION

The focal plane of the AXAF Imaging Spectrometer (ACIS) is populated with 10 Charge Coupled Devices (CCD) which convert incoming X-ray photons into electric signal and allow to get images of the X-ray sources simultaniously supplying information about the spectral composition of the input flux. The spectral structure of the celestial sources is very complicated and in order to succesfully deconvolve the source spectrum from the output signal of a CCD it is very important to have a high fidelity model of the device response.

We have developed a detailed model of the frontside illuminated CCD response to the X-ray illumination. The model is based on the most common approach for multipixel detectors sumulation (see, for instance,[1]) in which the photons of given energy are thrown into the random positions on the CCD surface and the device reaction is calculated for each individual photon. The procedure is then repeated many times to produce a histogram of the device response. Some blocks of our model, such as electron cloud diffusion in both depleted and undepleted bulk, charge cloud splitting between the pixels, event finding procedures, are similar to the ones described before in[1–3] and we will not discuss them in detail. In this work we will focus on the new developments in the device physics which allowed us to produce a model that is more adequate to the stringent calibration requirements of AXAF. The most important new features of our model are discussed below.

2. ABSORPTION IN THE GATE STRUCTURE

The gate structure of the ACIS CCD consists of the thin layers of polysilicon, silicon dioxide, and silicon nitride. X-ray photon can be absorbed in any of these layers with an exponentially distributed (depthwise) probability of interaction. To model this process the simulation program generates an exponentially distributed random number R. If $R > \frac{d}{\lambda}$ we assume that the photon have passed the layer of thicknness d with characteristic absorption length λ without being absorbed. Otherwise the photon is absorbed inside the layer.

The cross-section of the gate structure of the ACIS CCD along the direction of charge transfer is shown schematically on Fig. 1. It shows the details of the gate structure which were measured experimentally with Scanning Electron Microscope (SEM). Another cross-section, perpendicular to the direction of the charge transfer is shown on Fig. 2.

Absorption of X-rays in the gates becomes a very significant factor at low energies (below 1 keV) and immediately above silicon edge. Our model simulates all the details of the gate structure shown in Figures 1,2, such as gate overlaps,

---

Corresponding author G.P.; e-mail: gyp@space.mit.edu

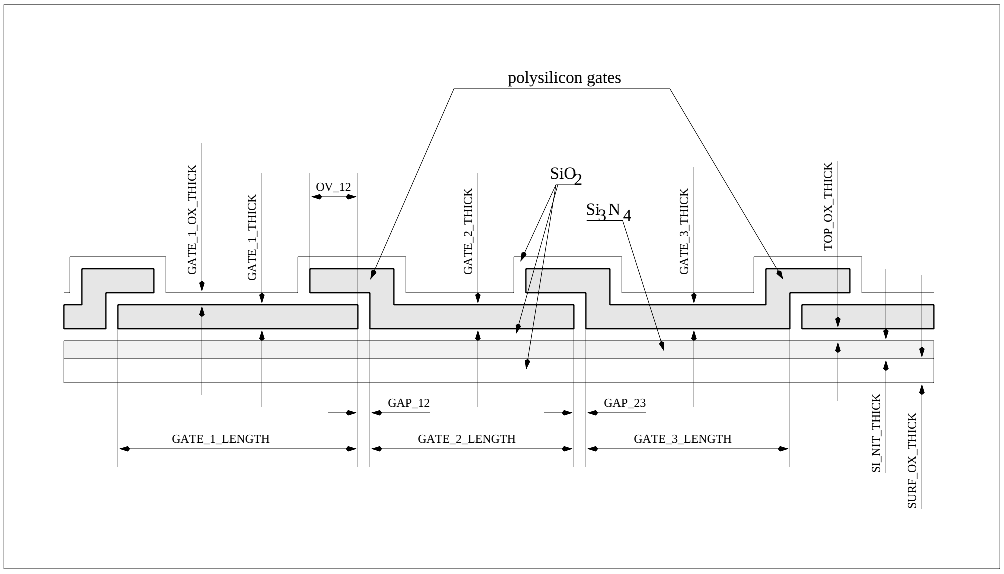

Figure 1. Cross section of the gate structure of the CCD along the transfer channel.

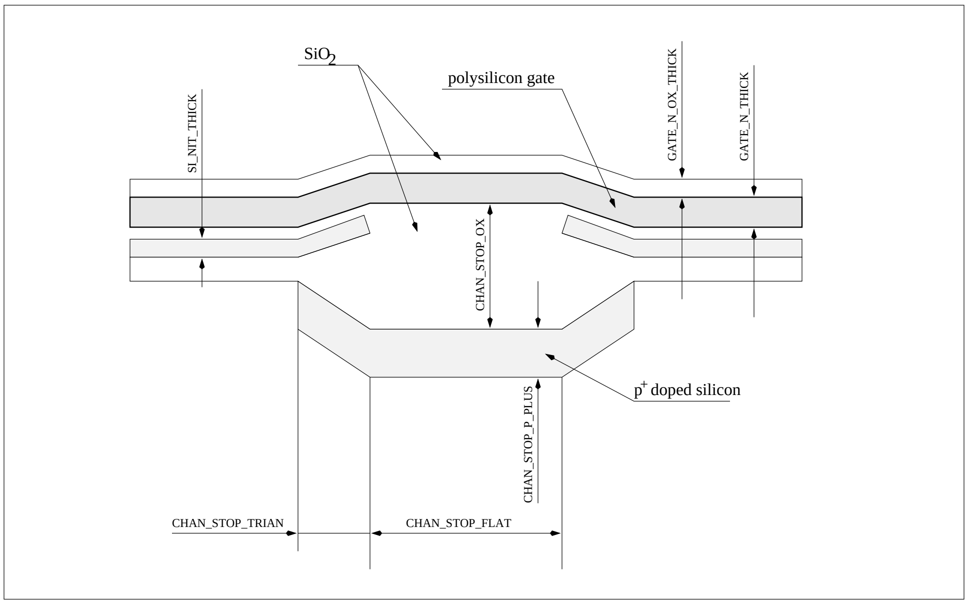

Figure 2. Cross section of the gate structure of the CCD perpendicular to the transfer channel.

oxide walls at the edges of the polysilicon gates, triangular shape of the wings of the oxide layer above the channel stop regions.

Characteristic absorption lengths for all the constituent layers are calculated based on the high precision measurements of the thin films of the corresponding materials performed at synchrotron beamlines (detailed description of these measurements can be found in [4,5]). As a result the model can very accurately predict quantum efficiency of the device in the entire energy range. It has a capability to show the distribution of the intensity of the detected flux across the pixel, which can be important for the subpixel resolution studies. Figures 3 and 4 demonstrate variations in sensitivity inside the pixel (this is a cross-section along the transfer channel at two different energies, immediately below the oxygen absorption edge and immidiately above it.

Slightly different gate thicknesses (in addition to the SEM measurement, their values were determined in the

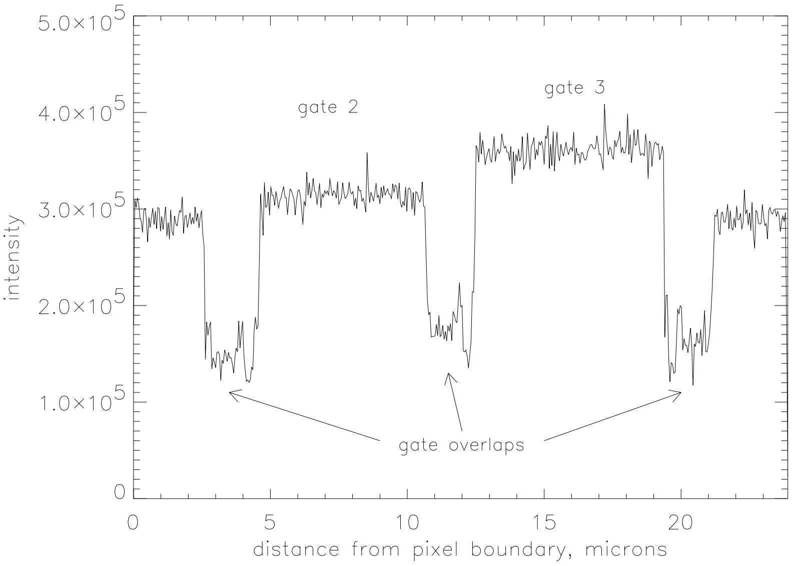

Figure 3. Number of detected events as a function of coordinate inside a single pixel. Energy of the incident photons is 525 eV, below oxigen absorption edge.

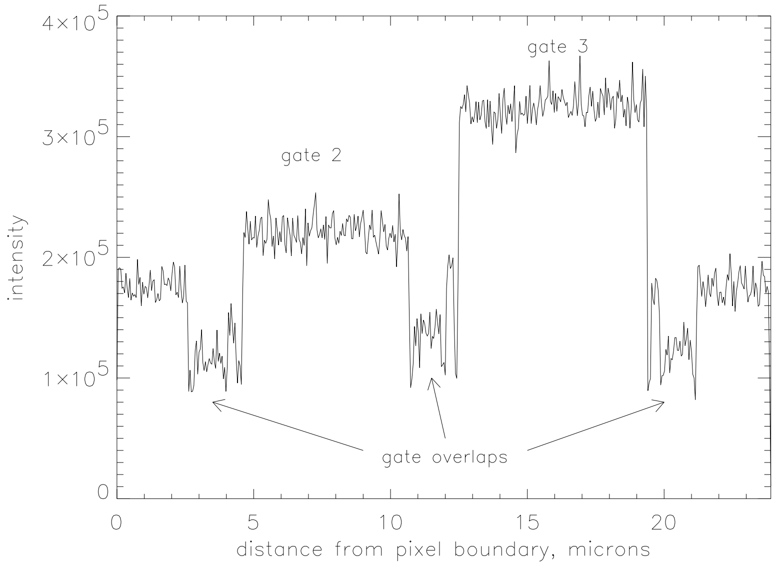

Figure 4. Number of detected events as a function of coordinate inside a single pixel. Energy of the incident photons is 539 eV, right above oxygen K edge. Notice a different behavior inside overlap regions

experiment where a mesh with 1.5 microns holes was put on the CCD surface, see[6]) result in different intensity under each of the gates. Sharp drops in the sensitivity can be seen in the regions where adjacent gates overlap. Silicon dioxide is less opaque than silicon below oxygen absorption edge and more opaque immediately above the edge. As a result, jumps in sensitivity corresponding to oxidized edges of the gates inside overlap regions go in opposite directions at the two energies.

3. ESCAPE AND FLUORESCENT PEAKS

Simulating CCD response we assume that for each photon with energy greater than the silicon absorption K edge (1839 eV) absorbed inside silicon, there is a 0.043 probability to emit a fluorescent photon with the characteristic energy of 1.739 keV. We neglect fluorescence from the other elements (oxygen and nitrogen) as well as fluorescence from the L-shell of silicon due to a very small probabilities of these events. The fluorescent photons are emitted uniformly in all directions and the program calclulates the spacial angles using random number generator. After that the absorption probability for the fluorescent photons is calculated in the same manner as for a primary photon. If the fluorescent photon leaves silicon substrate or interacts several pixels away from the site of interaction of the primary photon, an escape event will be detected. The model makes an accurate prediction of the escape peak amplitude.

An amplitude of the fluorescent peak was much harder to reproduce. The key to the correct model of the flourescent peak, especially at energies close to the *Si* absorption edge, is taking into account fluorescence from the gates. Immediately above *Si* edge absorption in the polysilicon gates becomes a significant factor. 4.3% of the absorbed photons produce a fluorescent photon and roughly half of them goes into the bulk of silicon and gets detected, while another half is emitted into the upper hemisphere and is lost. Unlike flourescent photons that are emitted from the bulk silicon, the leftover charge corresponding to the difference in energy between primary and fluorescent photon cannot be detected when it is formed in the polysilicon gate. This means that approximately half of the photons fluoresced from the gates will be found in the fluorescent peak, while only a tiny fraction of the ones fluoresced from the bulk will end up in the fluorescent peak. Because of this flourescence from the gates is by far a dominant factor in forming the flourescence peak at energies close to the *Si* K edge. On Fig. 5 are shown the amplitudes of the escape and flourescence peaks both from experimental data and simulated eventlists. Solid lines on Fig. 5 show the model predictions. The experimental results shown here came from the data collected at an electron storage ring at BESSY using Crystal Monochromator Beamline.

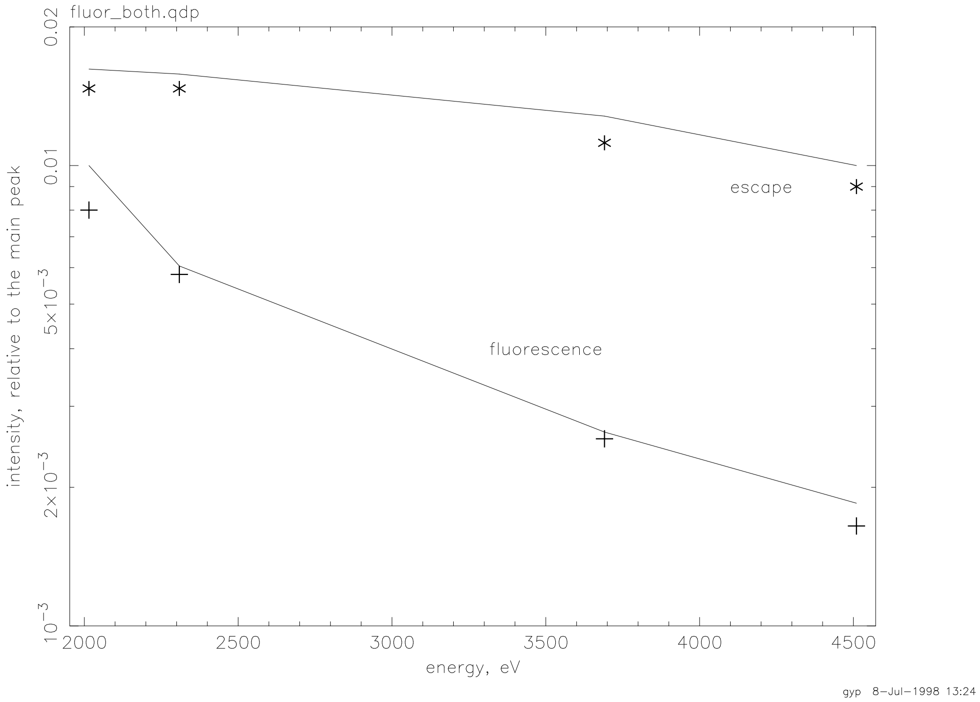

Figure 5. Intensities of experimentally measured escape (*) and fluorescence (+) features as a function of energy. Solid lines are the model predictions.

As it can be seen in the plot, the model provides a good agreement with the experimental data.

4. FORMATION AND DIFFUSION OF AN ELECTRON CLOUD

When the photon interacts with a silicon atom in a detector an electron cloud is formed. If the interaction occured in the depleted layer of silicon, the electrons are pulled by an electric field and the cloud drifts into the CCD potential wells, spreading wider due to the diffusion process at the same time. If the cloud was formed in the undepleted bulk of silicon, the electrons spread out without drifting component, the ones that reach the border with the depleted region are carried by the electric field into the potential wells of the CCD. The final cloud size is an important parameter which determines how the electron cloud is split between adjacent pixels. We use the most common approach and calculate the final cloud radius r according to the formula $r = \sqrt{r_i^2 + r_d^2}$, where r_i is initial cloud radius, r_d - cloud radius due to the diffusion process. To calculate the diffusion radius for charge generated both in depleted and undepleted bulk we follow the paper of Hopkinson.[3] For the initial cloud radius we use the results of Scholze&Ulm[7] if the interaction of the photon with the silicon atom did not occur near the $Si - SiO_2$ interface. Events which originate within a small distance from the surface lose some charge to the oxide layer and form a low energy tail of the response function. The treatment of such events is described in the following section 5, the original cloud radius for them being much smaller than for the bulk events.

5. LOW ENERGY TAIL

We have shown[8] that the low energy tail of the response function is formed by the photons that interact in close vicinity of the $Si - SiO_2$ interface. To illustrate this on Fig. 6 is shown a typical experimental histogram of the device response at 1700 eV. A low energy peak at approximately 50 ADU has its origin from the photons that interact inside the SiO_2 layer of the gate insulator structure. The most conclusive proof of this comes from the fact that the number of counts in the low energy peak is consistent with the calculated number of interactions inside the SiO_2 layer at different energies, as it is shown on Fig. 7. A remarkable feature of this plot is that the relative number of counts in the low energy peak jumps up sharply at 1846 eV, the energy which corresponds to the silicon absorption edge in SiO_2, which is different from the silicon absorption edge in the crystalline silicon. We have shown[5] that there exists a 6 eV difference between the silicon absorption edge energies in Si and SiO_2 and the jump at 1846 eV is a clear indication to the SiO_2 origin of the peak.

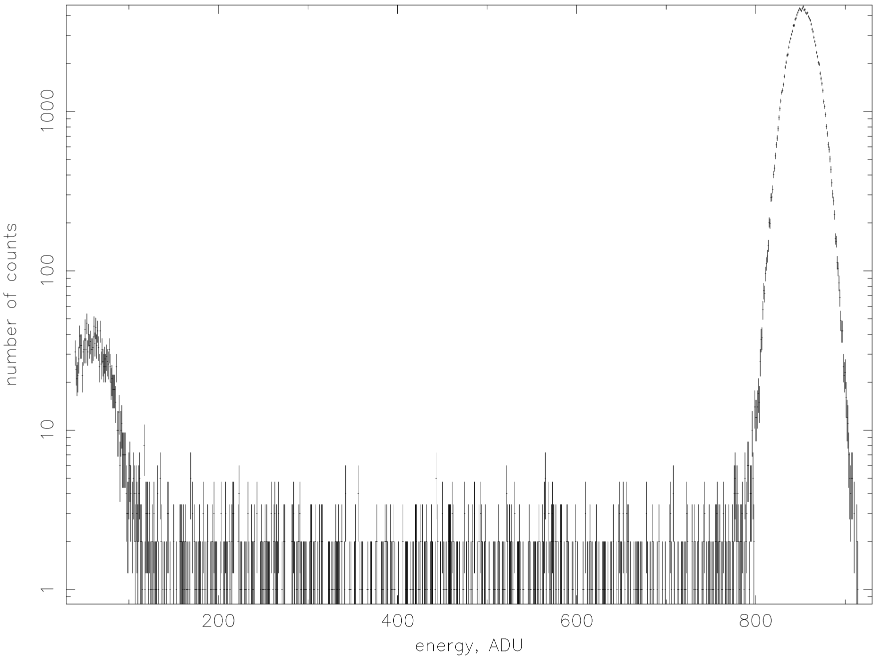

Figure 6. Histogram of the CCD response to 1700 eV X-rays.

Our general scheme of modeling the events which occur in SiO_2 or close to the $Si - SiO_2$ interface is shown on Fig. 8. According to it, electron clouds that are formed close to the interface are split between silicon and silicon dioxide and form the flat part of the tail. Our basic assumption when configuring the charge splitting is that the electron cloud is spherical and the number of electrons produced in each material is proportional to the volume of the corresponding segment of the sphere. We deduced the from the low energy peak position an effective electron-hole pair creation energy in SiO_2 of approximately 52 eV. This value contains in it electron losses both in SiO_2 and at the interface and, thus, is much higher than the reported value of 18 eV/pair. The diameter of the electron cloud sphere near the surface of silicon was determined from the experimental data (see[8]) and is much smaller than in the bulk due to the presence of the electric field repelling electrons away from the surface. Since we use parameters determined from the experimental data, the model produces a good agreement between simulated and experimental shape of the low energy tail.

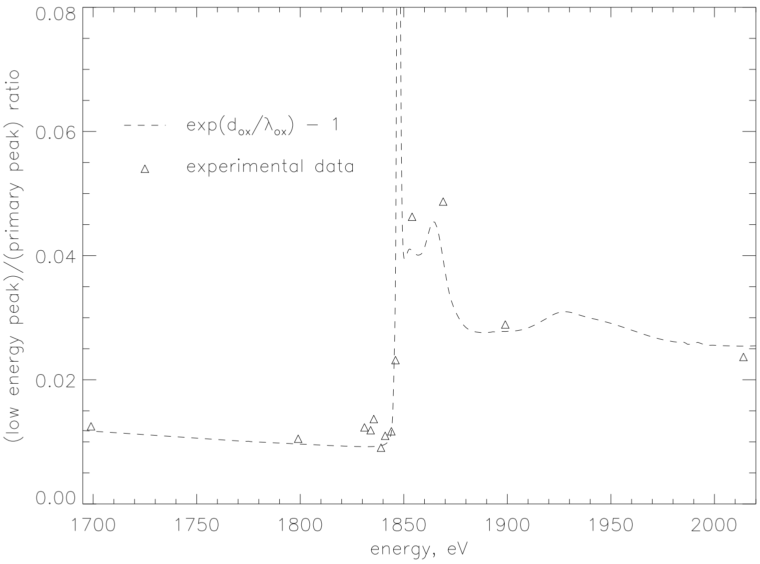

Figure 7. Ratio of number of counts in low energy peak and in the primary peak as a function of energy, calculated (dashed line), and measured (triangles).

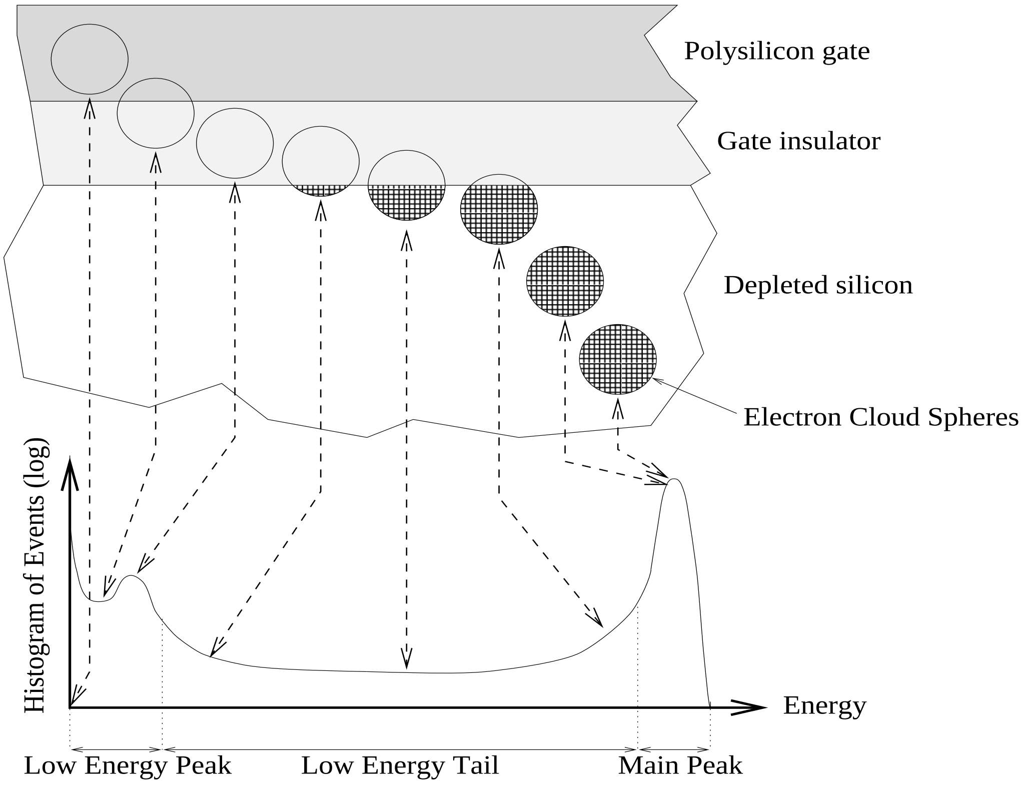

Figure 8. Scheme of forming low energy tail from the electron clouds generated close to $Si - SiO_2$ interface.

6. CHANNEL STOP EVENTS

A different procedure is used for the charge clouds that are formed in the doped area of channel stops. We have shown (see[9]) that events originating in the p^+ region of the channel stop suffer a charge loss and as a result form a shoulder at the low energy side of the main peak. Since the majority of the events in the channel stops is split between two adjecent pixels, this effect is most pronounced for the horisontally split events. A histogram of the horizontally split events (ASCA grades 3 and 4) at 1487 eV is shown in Fig. 9. Similarly to what was done for the low energy peak, we have measured a fraction of the events in the shoulder relative to the total number of counts in

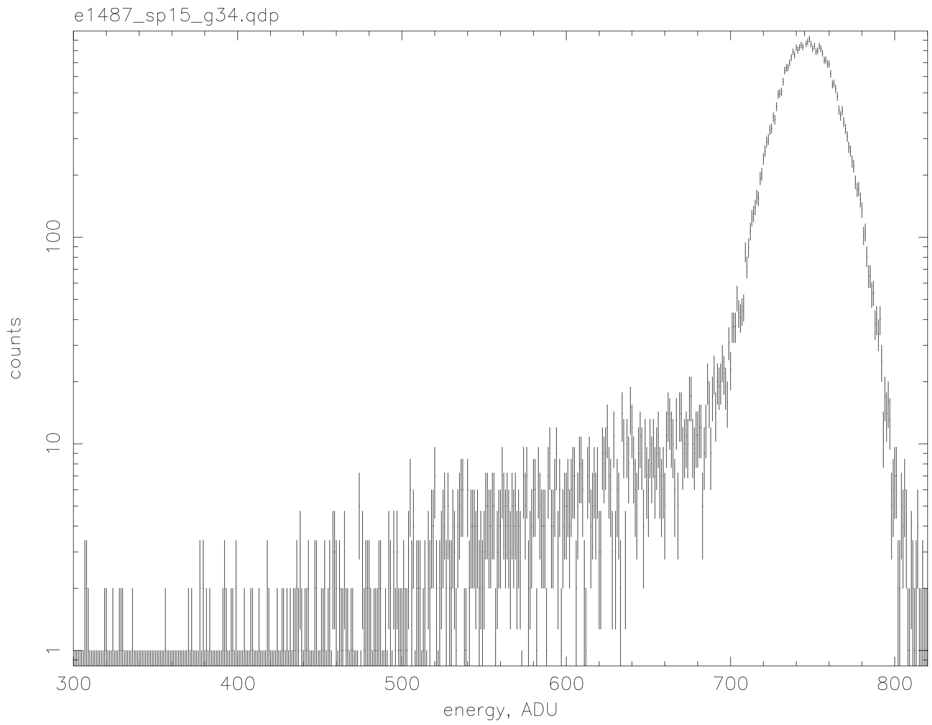

Figure 9. Histogram of the horizontally split events at 1487 eV

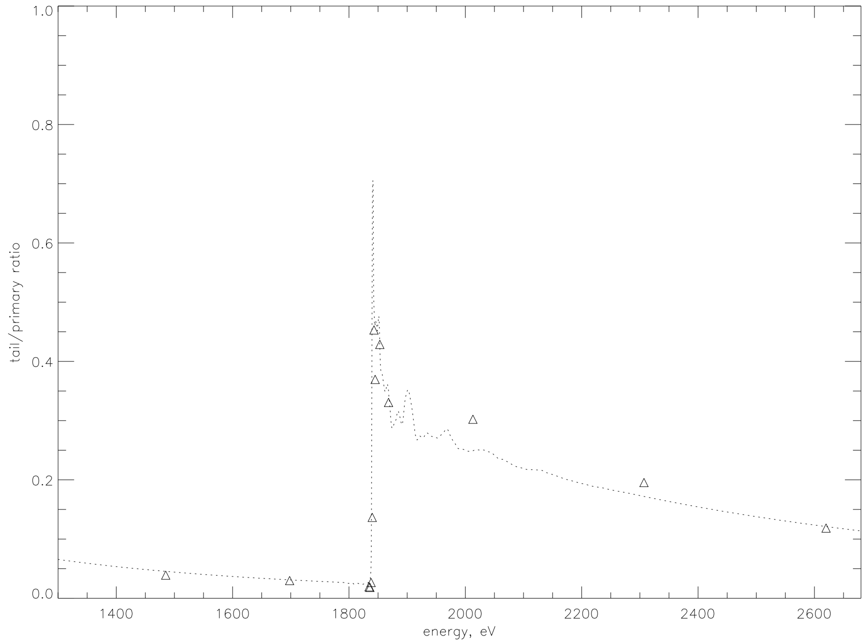

Figure 10. Ratio of the number of events in the shoulder to the total number of events in the horizontally split event histogram (triangles). Dotted line shows the calculated ratio assuming these events come from a layer of silicon 0.3 microns thick.

the horizontally split histogram as a function of energy. The corresponding plot shown on Fig. 10 indicates that all the lossy events in the channel stop area come from a shallow region of silicon close to the surface, since the silicon edge jump occurs at the energy corresponding to the absorption edge in the crystalline silicon. The depth of the region is approximately 0.3 microns. This is a havily doped p^+ region, shown as a shaded area on Fig. 2.

In order to account for the losses of charge in the p^+ area, for all the charge clouds having their centers inside this region we introduce an adjustable loss, which is proportional to the cloud charge. As a result our model can reproduce low energy tail of the horizontally split events.

7. SPLITTING OF CHARGE BETWEEN PIXELS AND WRITING TO AN OUTPUT FILE.

Once the cloud sizes and cloud centers are known, the final calculations are fairly common for this kind of model. The cloud is split between adjacent pixels assuming gaussian distribution of charge density in the cloud. This implies a simple routine for evaluating of the signal amplitude in the pixels adjecent to the cloud center. After that a readout noise with gaussian distribution is added to each pixel and the gain factor is introduced to adjust the amplitude of the signal to that of the paticular device that is being modeled. The last stage is an event finding routine – a procedure identical to the one used in the data analysis software to determine whether the amplitude of event is big enough to be written down into an eventlist. The output of the program is a standard eventlist which is entirely compatible with numerous software tools available for the real data analysis.

On Figures 11 and 12 are shown standard grade histograms for the experimental data taken under monochromatic illumination at 4510 eV and the simulated histograms for the same energy. While there are some discrepancies, the model reproduces all the important features of the experimental histogram, and the agreement between the model and the data in general is reasonably good.

8. ACKNOWLEDGEMENTS

This work was performed as part of the AXAF calibration program and was funded by NASA through contract NAS8-37716.

REFERENCES

1. K. McCarthy, A. Owens, A. Holland, and A. Wells, "Modelling of the X-ray response of CCDs," *Nuclear Instruments and Methods in Physics Research A* **362**, pp. 538–546, 1995.
2. J. Janesick, T. Elliott, S. Collins, T. Daud, D. Campbell, and G. Garmire, "Charge coupled device advances for X-ray scientific applications in 1986," *Optical Engineering* **26**, pp. 156–166, 1987.
3. G. Hopkinson, "Analytic modeling of charge diffusion in charge-coupled-device imagers," *Optical engineering* **26**, pp. 766–772, 1987.
4. G. Prigozhin, J. Woo, J. Gregory, A. Loomis, M. Bautz, G. Ricker, and S. Kraft, "Quantum efficiency of X-ray CCDs," *SPIE Proceedings, Solid State Sensor Arrays:Development and Applications* **3301**, pp. 108–115, 1998.
5. G. Prigozhin, J. Woo, J. Gregory, A. Loomis, M. Bautz, G. Ricker, and S. Kraft, "X-ray absorption near edge structure in quantum efficiency of X-ray CCDs," *Optical Engineering* **37**, 1998.
6. M. Pivovaroff, S. Jones, M. Bautz, S. Kissel, G. Prigozhin, G. Ricker, H. Tsunemi, and E. Miyata, "Measurement of the subpixel structure of AXAF CCD's," *IEEE Transactions on Nuclear Science* **45**, pp. 164–175, 1998.
7. F. Scholze and G. Ulm, "Characterization of a windowless Si(Li) detector in the photon energy range 0.1-5 keV," *Nuclear Instruments and Methods in Physics Research A* **339**, pp. 49–54, 1994.
8. G. Prigozhin, S. Jones, M. Bautz, and G. Ricker, "Physics of the low energy tail in the ACIS CCD. The spectral redistribution function.," *Nuclear Instruments and Methods in Physics Research A, submitted* , 1998.
9. G. Prigozhin, "X-ray detection in channel stops," *MIT ACIS memo #150* , 1998.

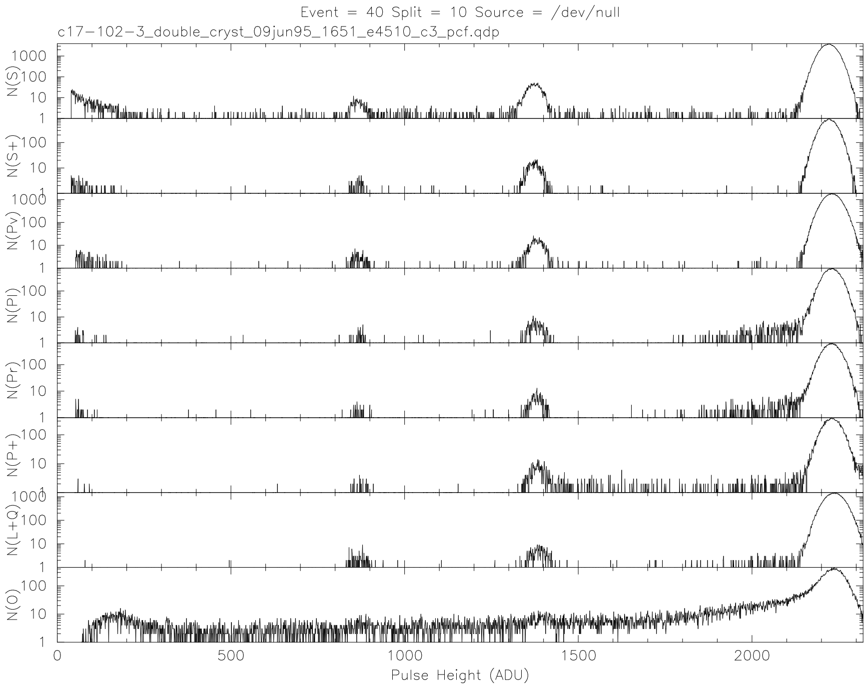

Figure 11. Standard graded histograms for experimental data taken with a monochromatic source at 4510 eV.

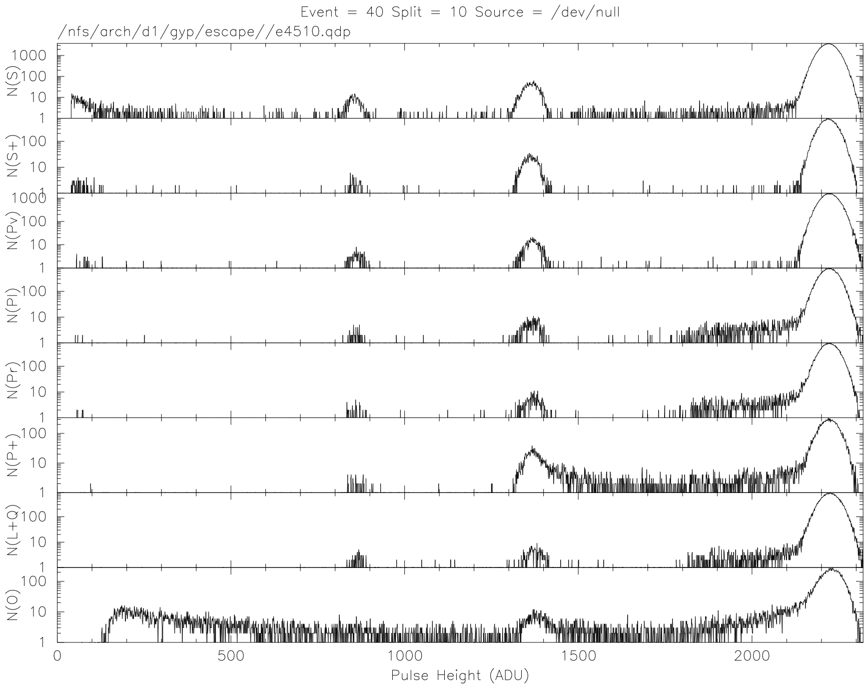

Figure 12. Standard graded histograms showing simulated response to 4510 eV X-rays.